

Antimalarial activity of cupredoxins: the interaction of *Plasmodium* Merozoite Surface Protein 1₁₉ (MSP1₁₉) and Rusticyanin*

Isabel Cruz-Gallardo¹, Irene Díaz-Moreno¹, Antonio Díaz-Quintana¹, Antonio Donaire², Adrián Velázquez-Campoy³, Rachel D. Curd⁴, Kaveri Rangachari⁴, Berry Birdsall⁵, Andres Ramos⁵, Anthony A. Holder⁴ and Miguel A. De la Rosa¹

¹From the Instituto de Bioquímica Vegetal y Fotosíntesis (IBVF), cicCartuja, Universidad de Sevilla – CSIC, Avda. Américo Vespucio 49, Sevilla 41092, Spain.

²Departamento de Química Inorgánica, Facultad de Química, Universidad de Murcia, Campus Universitario de Espinardo, Murcia 30100, Spain.

³Instituto de Biocomputación y Física de Sistemas complejos (BIFI), Universidad de Zaragoza, C/ Mariano Esquillor, Zaragoza 50018, Spain.

⁴Parasitology Division, MRC National Institute for Medical Research, The Ridgeway, Mill Hill, London NW7 1AA, UK.

⁵Molecular Structure Division, MRC National Institute for Medical Research, The Ridgeway, Mill Hill, London NW7 1AA, UK.

*Running title: *MSP1₁₉ – Rusticyanin Complex*

To whom correspondence may be addressed: Professor Miguel A. De la Rosa. Instituto de Bioquímica Vegetal y Fotosíntesis (IBVF), cicCartuja, Universidad de Sevilla – CSIC, Américo Vespucio 49, 41092 Sevilla, Spain. Tel.: 34-954489506; Fax.: 34-954460065; E-mail: marosa@us.es

Keywords: malaria, *Plasmodium*, MSP1₁₉, rusticyanin, NMR, ITC

Background: The interaction of MSP1₁₉ with the cupredoxin azurin inhibits the growth of *Plasmodium falciparum* in red blood cells.

Results: Rusticyanin forms a well-defined complex with MSP1₁₉ upon binding at the same surface area than inhibitory antibodies.

Conclusion: Rusticyanin becomes an excellent therapeutic agent for malaria.

Significance: Knowing the rusticyanin-MSP1₁₉ interface will allow the design of novel anti-malarial drugs.

SUMMARY

The discovery of effective new antimalarial agents is urgently needed. One of the most frequently-studied molecules anchored to the parasite surface is the merozoite surface protein-1 (MSP1). At red blood cell invasion MSP1 is proteolytically processed and the 19 kDa C-terminal fragment (MSP1₁₉) remains on the surface and is taken into the red blood cell, where it is transferred to the food vacuole and persists until the end of the intracellular

cycle. Since a number of specific antibodies inhibit erythrocyte invasion and parasite growth, MSP1₁₉ is therefore a promising target against malaria. Given the structural homology of cupredoxins with the F_{ab} domain of monoclonal antibodies, an approach combining NMR and ITC measurements with docking calculations based on BiGGER is employed on MSP1₁₉-cupredoxin complexes. Among the cupredoxins tested, rusticyanin forms a well-defined complex with MSP1₁₉ at a site that overlaps with the surface recognized by the inhibitory antibodies. The addition of holo-rusticyanin to infected cells results in parasitemia inhibition, but negligible effects on parasite growth can be observed for apo-rusticyanin and other proteins of the cupredoxin family. These findings point to rusticyanin as an excellent therapeutic tool for malaria treatment and provide valuable information for drug design.

Malaria is a widely-spread disease causing morbidity and mortality throughout a large part of the world. The increasing resistance of *Plasmodium falciparum*, the causative agent of the most deadly form of the disease, to current drugs has only increased the urgency for finding new anti-malarial agents (1,2), including an effective vaccine and new drug therapies (3,4). There are five *Plasmodium* species that infect humans, while others infect other primates or rodents. Among this latter group, rodent parasites such as *Plasmodium yoelii* provide useful laboratory models for the study of malaria. The disease is caused by the replication and multiplication of the asexual blood stages in red blood cells. The merozoite form of the parasite invades the host cell, where it develops and replicates to form several new merozoites that then burst out of the cell to continue the cycle of invasion and multiplication. The invasion of red blood cells requires an initial recognition and binding mediated by parasite surface ligands, followed by reorientation and the formation of a moving junction between the erythrocyte and merozoite surfaces as the parasite enters the cell. Merozoite surface protein-1 (MSP1)⁶ has been implicated in this initial binding between parasite and host cell.

Located on the surface of the asexual blood-stage schizont and merozoite, MSP1 is one of the most frequently-studied molecules of the parasite (5). It is synthesized as a ~200-kDa precursor attached to the surface of the parasite via a glycosylphosphatidylinositol (GPI) anchor, which undergoes a two-step proteolytic process: first, at merozoite release and, then, at erythrocyte invasion (6). As a result of this processing, the MSP1 is cleaved into several polypeptides that are shed from the surface in the final processing step, save a 19 kDa C-terminal fragment (MSP1₁₉). MSP1₁₉ is retained on the parasite surface by the GPI anchor and taken into the red blood cell at invasion (7-9). The role of MSP1₁₉ in the subsequent intracellular development of the parasite is poorly understood, although it is transferred to the developing food vacuole, where it remains until the end of the intracellular cycle, and is discarded in the residual body together with products of hemoglobin digestion such as hemozoin (10). MSP1₁₉ is considered a promising malaria vaccine candidate due to the abundant

evidence of specific antibodies inhibiting erythrocyte invasion and parasite growth, for instance, via the disruption of MSP1 proteolytic processing and intracellular parasite development (11).

At the structural and functional levels, MSP1₁₉ is particularly well-conserved among *Plasmodium* species (Figure 1) (12-17) and its three-dimensional structure has been shown to consist of two epidermal growth factor (EGF)-like domains in close contact. A characteristic disulphide-bridge pattern (Figure 1) makes MSP1₁₉ highly resistant to proteases (19) and may explain why MSP1₁₉ remains intact in the digestive food vacuole up to the end of the intracellular cycle (10).

MSP1-specific immunoglobulins react with conformational epitopes of MSP1₁₉. Some of these antibodies inhibit parasite invasion of erythrocytes, whereas others do not. Fine-structure epitope mapping of different monoclonal antibodies (mAbs) and the use of NMR methods indicates the binding of two inhibitory antibodies to epitopes on one side of the molecule near the interface between the two EGF domains, including residues from both domains (20,21). By contrast, non-inhibitory neutral mAbs bind elsewhere on the molecule (15, 20). Here we have used MSP1₁₉ from *P. yoelii*, a rodent malaria parasite used as a laboratory model for vaccine studies (22) and for which both inhibitory and neutral antibodies have been partially mapped on the structure (23, 24, Curd *et al.*, unpublished data). Independently of the immunoglobulin class, complexes involving MSP1₁₉ are kinetically rather stable with dissociation constants in the μM to sub-nM range (15, 25, Lock and Holder, unpublished data). As the binding affinity is similar in all cases, it has been assumed that the inhibitory effect depends mainly on steric factors – namely, epitope location – rather than the nature of the antibody.

The present study has been based on the structural homology of cupredoxins with the F_{ab} fragment of an antibody, as well as on reports of a protein from this family interacting directly with MSP1₁₉ and blocking the increase of parasitemia in human red blood cells infected by *P. falciparum*, suggesting a promising treatment (26,27). We first used DaliLite pairwise comparison program to identify structural similarities between cupredoxins and the Fab fragment

(28). A screening was then performed combining NMR and ITC measurements with docking calculations using BiGGER which indicated that, among the cupredoxins tested, rusticyanin (Rc) provided the most effective binding to MSP1₁₉. While the two proteins form a well-defined complex where Rc interacts at the interface between the two MSP1₁₉ sub-domains, at a site that overlaps with the surface recognized by the inhibitory antibodies, *P. falciparum* growth is inhibited by the presence of Rc in red blood cell cultures. Interestingly, the copper site plays a key role in complex formation, since apo-Rc is not only unable to interact with MSP1₁₉, but also to inhibit parasite invasion and development in infected red blood cells.

EXPERIMENTAL PROCEDURES

Expression and purification of proteins—*Plasmodium yoelii* MSP1₁₉ (¹⁵N-labeled or unlabeled) was produced [essentially as described previously (29)] from a synthetic gene optimized for *Pichia pastoris* expression using as nitrogen source either ¹⁵NH₄Cl or (NH₄)₂SO₄ for labeled and unlabeled protein, respectively. The 99-amino acid sequence corresponds to residues 1656-1754 of the UniProtKB entry P13828 containing the N-terminal tag HHHHHHIEGR that has little effect on the NMR spectrum (20). Secreted hexahistidine-tagged MSP1₁₉ was purified from the culture medium by nickel affinity chromatography (Ni Sepharose 6 Fast Flow, GE Healthcare) and according to a previously elaborated protocol (12).

All recombinant metalloproteins were expressed in *Escherichia coli* cultures in LB medium and purified according to previously-elaborated procedures, namely *Acidithiobacillus ferrooxidans* Rc (30, 31), *Nostoc* sp. PCC 7119, *Phormidium laminosum* and poplar plastocyanins (Pc) (32-34) and *Pseudomonas aeruginosa* azurin (Az) (35).

NMR spectroscopy— All protein samples were concentrated in 10 mM potassium phosphate (pH 6.5) using Millipore 3K NMWL centricons and microcons. MSP1₁₉ samples ranged in concentration from 0.5 to 2 mM, whereas cupredoxins were used in the range of 2 to 5 mM. All NMR samples contained 10% of D₂O to adjust the lock signal. Reduction of the metal center in samples of copper (I) cupredoxins was

achieved by adding sodium ascorbate, while oxidation of the metal center in samples of copper (II) proteins was achieved using sodium ferricyanide for Pc and Az, and sodium hexachloroiridate (IV) for Rc. In all cases, the proteins were extensively washed to remove the excess of the reducing/oxidizing agent.

NMR experiments were performed in a Bruker Avance 600 MHz spectrometer at 25 °C. The sequence-specific assignment of the backbone amide groups of ¹⁵N MSP1₁₉ (BMRB accession number: 19233) was achieved using standard backbone experiments (HNCACB, HNCA, etc.) and was confirmed using 3D ¹H-¹⁵N NOESY-HSQC and 3D ¹H-¹⁵N TOCSY-HSQC spectra. The interaction of MSP1₁₉ with cupredoxins was followed by acquiring two-dimensional ¹H-¹⁵N HSQC spectra during the titration of 0.5 mM ¹⁵N-MSP1₁₉ solutions with an increasing amount of oxidized or reduced cupredoxins up to a final cupredoxin:MSP1₁₉ molar ratio of 4:1. The pH value of the sample was verified after each titration step. Prolines, which are invisible resonances in ¹⁵N HSQC spectra, are located at the positions 4, 15, 50, 61, 84 and 86, whereas Gly1, Val2, Glu69 and Asn73 are unassigned residues. All data processing was performed with Bruker TopSpin 2.0, and NMR analysis of line broadening perturbations of the cupredoxin-bound MSP1₁₉ with respect to free malarial protein was performed in the SPARKY program (36).

NMR linewidth analysis— To estimate linewidths, the peaks were fitted to a Gaussian function for the ¹⁵N and ¹H dimensions using the program SPARKY with a 10,000 steps minimization and a 0.05% tolerance.

In the analysis of the linewidths ($\Delta v_{1/2}$), the overall broadening ($\Delta\Delta v_{1/2}$) obtained from signals displaying only minor line broadening was first subtracted from the linewidth of the corresponding signal. Then, for each residue, the differences of linewidths between free and interacting MSP1₁₉ were calculated in every titration series ($\Delta\Delta v_{1/2}^{\text{Binding}}$). The threshold value, used to identify a specifically broadened residue when data from the titration series were analyzed together, was defined as the average $\Delta\Delta v_{1/2}^{\text{Binding}}$ for the system plus 2 standard deviations ($2S_{n-1}$). The average $\Delta\Delta v_{1/2}^{\text{Binding}}$ and standard deviation were calculated for all amides with values \leq

10 Hz on the basis that data > 10Hz clearly indicated a specifically broadened residue and their inclusion would bias the average to a higher value.

Some assigned signals of the free MSP1₁₉ HSQC spectrum overlap (Val9, Asn87 and Cys95) or exhibit very low intensity (Gly41 and Asn42), so they could not be properly integrated to include them in the linewidth analysis.

ITC– All ITC experiments were performed using VP-ITC and Auto-ITC200 instruments (Microcal, GE Healthcare) at 25 °C titrating Rc with MSP1₁₉. The reference cell was filled with distilled water. The experiments consisted of 10-μL or 2-μL injections of 0.3 mM MSP1₁₉ solution in 10 mM potassium phosphate buffer pH 6.5 into the sample cell, initially containing 6.67 μM Rc solution - reduced, oxidized and apo forms - in the same buffer. All the solutions were degassed before the titrations were performed. Titrant was injected at appropriate time intervals to ensure the thermal power signal returned to the baseline prior to the next injection. To achieve homogeneous mixing in the cell, the stirring speed was kept constant at 1000 rpm in the Auto-ITC200 and at 450 rpm in the VP-ITC. The data, specifically the heat per injection normalized per mole of injectant vs. molar ratio, were analyzed with Origin 7 (Microcal) using a single-site binding model. Calibration and performance tests of the calorimeter were carried out conducting CaCl₂–EDTA titrations with solutions provided by the manufacturer.

Molecular Docking simulations– A soft docking algorithm implemented in the BiGGER software package (37) was used to determine *in silico* a model of the complexes MSP1₁₉-Az, MSP1₁₉-Pc and MSP1₁₉-Rc. The coordinates files of cupredoxins were 1JZG for Az (38), 1NIN for Pc (39) and 1A3Z for Rc (40). For each run, 5000 docking geometric solutions were generated based on the complementarity of the protein surfaces. These solutions were evaluated and ranked according to their “global score”, and different interaction criteria including electrostatic energy of interaction, relative solvation energy and the relative propensity of side chains to interact. For the MSP1₁₉-Rc adduct, NMR restraints were introduced in the docking calculations. All complexes graphic images were generated using the UCSF

Chimera package (www.cgl.ucsf.edu/chimera; 41).

***P. falciparum* cultures**– Synchronized *P. falciparum* 3D7 late stage trophozoites at 33–36h were used. The final parasitemia and hematocrit were between 0.1–0.2% and 2% respectively. Red blood cells used for the assay were centrifuged to remove the buffy coat and washed twice in RPMI 1640 medium so that no white blood cells were present. The culture medium contained RPMI 1640 supplemented with 5g/L albumax, 0.025g/L gentamycin, and 0.292g/L L-glutamine.

***P. falciparum* growth inhibition assay**– Sterile 96 well black tissue culture plates (Costar) were used routinely for every assay. The holo- or apo-species of Rc and *Nostoc* Pc were diluted in culture medium and used in duplicate wells for each dilution (200, 100, 50 and 25 μM, respectively) in a final volume of 100 μL per well. Two control sets were used in duplicate wells, one set with no added cupredoxin (positive control) and one with uninfected red blood cells (negative control). The plates were incubated at 37 °C for 48h in a gas chamber flushed with 5% CO₂, 5% O₂, and 90% N₂. After 48h, supernatants were removed from each well, replaced with fresh medium containing protein and incubated for a further 48h in the same manner. At the end of the 96h incubation, 25 μL of SYBR Green I dye (SYBR Green I nucleic acid gel stain 10000x, in DMSO from Invitrogen) in lysis buffer (1 μL dye to 1 mL lysis buffer) was added to each well and stored overnight at -20 °C. The lysis buffer contained Tris-HCl (20 mM, pH8.0), EDTA (2 mM), Saponin (0.16 % w/v) and Triton X-100 (1.6 % v/v). Plates were thawed at room temperature and fluorescence intensity was measured with a FLUO Star Omega microplate fluorescence reader (BMG Labtech). Values were expressed in relative fluorescence units. Binding of SYBR Green is specific for parasite DNA as mature erythrocytes lack DNA and RNA. Fluorescence intensity unit was converted to percentage (%) of growth as follows: % growth = (culture under Rc or Pc) – (uninfected RBC) / (culture with no Rc or Pc) – (uninfected RBC) x 100, where RBC are red blood cells.

RESULTS

Structural similarities between cupredoxins and the F_{ab} fragment of a mAb–

The F_{ab} fragment crystal structure of mAb G17.12 (15), shown to bind MSP1₁₉, is constituted of two domains, A and B, containing two regions, variable (symbolized by 1) and constant (symbolized by 2), with the canonical β -sandwich fold of the immunoglobulin superfamily (Figure 2A). Consistent with previous reports, the DaliLite pairwise comparison program (28) identified significant structural similarities between the A1 fragment of the mAb and copper-containing redox proteins with immunoglobulin fold, such as Az, Pc and Rc. In particular, the structural alignment between the A1 fragment and Az reveals a matching region, which is mainly localized at the two antiparallel β -sheets, as described previously (26; Figure 2B), and with a Dali Z-score of 2.9. For the two other cupredoxins, Pc and Rc, this structural match is extended to the loops connecting β strands yielding Z-scores of 3.1 and 2.6, respectively (Figure 2C).

Given the structural similarity between various cupredoxins and the F_{ab} fragment, *ab initio* docking approaches were performed with no experimental restraints (Figure 3) to explore the capability of the metalloproteins to interact with MSP1₁₉ from *P. yoelii*. MSP1₁₉ is well-conserved among the species with more than 50% sequence identity (Figure 1A), with conserved three-dimensional structure and common functional features (17). We used the BiGGER rigid docking algorithm to generate sets of possible orientations for the different cupredoxin probes around MSP1₁₉ (the target). Figure 3 shows the distribution of MSP1₁₉ mass centers resulting from the 100 best solutions from each computation around the corresponding copper protein. For Az and Pc, we observe a remarkably broad dispersion of the MSP1₁₉ geometry centers, suggesting the lack of specific surface complementarity. By contrast, molecular docking for the Rc-MSP1₁₉ interaction indicates that MSP1₁₉ explores a well-defined area of Rc surrounding its copper center.

MSP1₁₉ interactions with cupredoxins by NMR– The MSP1₁₉-cupredoxin interaction was monitored by recording 2D ¹⁵N-HSQC NMR spectra on ¹⁵N MSP1₁₉, both free and following the addition of Az, Pc or Rc. The absence of changes in MSP1₁₉ resonances – either chemical shift perturbations or line broadening – indicates no detectable binding

to Az and Pc in any of their oxidation states (Figure 4, *upper* and *middle* panels). By contrast, linewidth changes of certain MSP1₁₉ amide signals upon addition of Rc(Cu¹⁺) suggest a specific MSP1₁₉-Rc interaction (Figure 4, *lower* panel). Such observations coincide with *ab initio* docking simulations performed (Figure 3) which suggested a well-defined complex only between Rc and MSP1₁₉.

To probe in greater detail the interaction of MSP1₁₉ with either oxidized or reduced Rc, we analyzed the linewidths of MSP1₁₉ resonances from ¹⁵N-HSQC spectra across several titrations. Binding to Rc results in general signal broadening due to the increase in the rotational correlation time of MSP1₁₉ when interacting with Rc. In addition, several MSP1₁₉ backbone amides clustered in one area of the structure undergo larger changes in linewidths ($\Delta\Delta v_{1/2}^{\text{Binding}}$) upon Rc binding (Figure 5, Figure 6). These resonances are expected to be at or in the proximity of the area of MSP1₁₉ interacting with Rc. In order to selectively define resonances most likely to be part of the interface, threshold values – specifically, $\Delta\Delta v_{1/2}^{\text{Binding}} \geq 5\text{Hz}$ for ¹⁵N and $\geq 11\text{Hz}$ for ¹H dimension – were set (Experimental Procedures). As expected, the distribution of linewidth changes ($\Delta v_{1/2}$) becomes broader as the Rc:MSP1₁₉ ratio increases (data not shown).

At the Rc(Cu¹⁺):MSP1₁₉ ratio of 1.5:1, 14 amino acids show considerable ¹⁵N linewidth changes in MSP1₁₉ HSQC spectra (Figure 5A and 5B). These residues are mainly distributed along two regions of MSP1₁₉, namely, at the beginning of N-terminal EGF domain involving Asp3, Lys5, His6, Val7, Asp10 and at the end of C-terminal domain comprising Thr85, Ala88, Tyr89, Phe94, Ser97. In addition, Asp24, Asp25 and Arg31 at the two first antiparallel β -strands, along with Cys59, are also altered. Figure 5C shows the map of MSP1₁₉ residues affected by Rc addition, with colors corresponding to line broadening in the ¹⁵N dimension. The sequential stretches of residues detailed above form the main cluster on the MSP1₁₉ surface, which surrounds the two EGF domain interface. Interestingly, some of these affected residues – Asp24, Asp25, Arg31 and Cys59 – are located at the rear of the protein (Figure 5C). While Asp24 and Asp25 are close to amino acids at the N-

terminal, Arg31 and Cys59 lie near Phe94. Since these four residues are adjacent to others placed at the EGF domain interface and involved in direct contact with Rc, these linewidth perturbations are probably a secondary effect of binding. Similar conclusions may be inferred from ¹H linewidth analysis, although protons are more sensitive to broadening (data not shown).

NMR titration of oxidized Rc on MSP1₁₉ results in significant MSP1₁₉ linewidth perturbations at a Rc(Cu²⁺):MSP1₁₉ ratio of 4:1, at which some signals broaden beyond the detection limit (Figure 6A). The MSP1₁₉ resonances affected by Rc(Cu²⁺) binding involve both N-terminal (Asp3, Lys5, Asp10, Asp13) and C-terminal (Cys79, Thr85, Tyr89, Gly92, Phe94, Ser97, Ser98) regions, as described for the reduced system at a Rc(Cu¹⁺):MSP1₁₉ ratio of 1.5:1. An additional stretch (Phe21-Asp24, Gly26, Glu29, Arg31 and Cys59) is also perturbed while His6, Val7, Asp25 and Thr27 were residues over the detection limit (Figure 6A). Notably, the strength of the broadening observed for a 4:1 Rc(Cu²⁺):MSP1₁₉ ratio is comparable to the one observed at a 1.5:1 Rc(Cu¹⁺):MSP1₁₉ ratio, indicating that MSP1₁₉ bind more weakly to the oxidized Rc. However, the MSP1₁₉ interacting surface involved in Rc recognition at a Rc:MSP1₁₉ ratio of 4:1 is independent of the cupredoxin redox state (Figure 6).

Binding of MSP1₁₉ to holo-Rc by ITC—ITC measurements reveal that MSP1₁₉ binds to Rc either in its reduced or oxidized state with a 1:1 stoichiometry at 25 °C (Figure 7). Notably, the interaction of MSP1₁₉ with Rc(Cu¹⁺) is exothermic with a dissociation affinity constant (K_d) of 2 μM, whereas that with Rc(Cu²⁺) is an endothermic process with lower binding affinity ($K_d = 25$ μM) (Table 1). Such differences in K_d values are in agreement with NMR titrations and suggest that MSP1₁₉ binds to reduced Rc with a greater affinity than to oxidized Rc. Further experiments need to be performed to explain the opposite sign in the enthalpy of both processes as it could be related to (i) changes in the protonation/deprotonation equilibrium of ionizable groups of the interacting proteins; (ii) variations in the hydrogen-bonding networks; (iii) differences in water arrangement in the vicinity of oxidized or reduced cofactors; and (iv) slight

conformational modifications altering the number of solvent molecules excluded from the protein interface.

The case of apo-Rc—To determine the role of the copper center, NMR and ITC titrations were carried out using MSP1₁₉ and apo-Rc. Surprisingly, NMR titrations showed no substantial linewidth changes even at an apo-Rc:MSP1₁₉ ratio of 4:1 (Figure 8). The finding was further corroborated by ITC measurements, as the weak calorimetric profile suggests a lack of interaction (Figure 8). Altogether these data indicate the relevance of the copper center in the binding to MSP1₁₉. Despite the small structural differences in cupredoxins reported previously in solid state, there exists a high degree of mobility of the metal-binding loops in solution in the apo form, as recently demonstrated by NMR (42,43). The different pattern between apo and holo-Rc versus MSP1₁₉ could be related with the found differences in the dynamics of this site in the two forms.

Docking simulations with BiGGER—Along with the *ab initio* docking calculations run on the MSP1₁₉/Rc(Cu¹⁺) complex, revealing how the MSP1₁₉ mass center docks on the Rc metal crevice (Figure 3), an NMR-restrained docking with BiGGER was also performed. Linewidth data for those MSP1₁₉ residues in contact with Rc at a Rc:MSP1₁₉ ratio of 1.5:1 were included in the run. The output is a set of docked solutions that can be ranked according to the BiGGER global score or individual scores, such as hydrophobic criteria, electrostatics and geometrical parameters. Figure 9 shows the best 100 solutions, as represented by Rc geometry centers, according to the global and hydrophobic scores from the program (Figure 9A). The best-scoring models predicted by restrained docking reveal how MSP1₁₉ leans its EGF-domain interface to approach Rc (Figure 9A). Indeed, the proximity of the surfaces on both proteins in the complex is shown in the space-filling representation (Figure 9A). In addition to the copper center, loops connecting Rc β-strands are in close contact with MSP1₁₉. A deep analysis of the complex interface predicted by docking points to the N-terminal and C-terminal regions of the MSP1₁₉ as driving complex formation as some NMR restraints are satisfied (Figure 9B). In the model reported, some electrostatic

interactions occur (Figure 9C) since Rc residues Lys81 and Lys116 are close to Glu91 and Glu83 in MSP1₁₉. Furthermore, Lys5 of MSP1₁₉ can interact with Glu9 of Rc, although the Glu is partially buried. The Rc interaction surface is mainly hydrophobic with the exception of a single positive spot, Lys81 and Lys116, surrounded by Phe83, Gly82 and Trp7 and the copper center, which, in turn, is enclosed by Met99, Val98 and Pro141. This interaction mode resembles those of the copper protein Pc and cytochrome *c*₆ (*Cc*₆) with their photosynthetic partners, cytochrome *f* and photosystem I. In such complexes, Pc and *Cc*₆ use the hydrophobic site surrounding the copper center and the heme group – site 1 – as well as their charged patch (site 2; 44,45).

Inhibition of *P. falciparum* growth by holo-Rc– To assess the physiological relevance of the MSP1₁₉ binding to Rc, the growth of *P. falciparum* – within red blood cells – was followed in the presence of either holo- or apo-Rc (Experimental Procedures). The addition of holo-Rc to infected cells resulted in parasitemia inhibition, as culture growth decreased significantly (Figure 10) at a concentration of 100 μM till the point of complete inhibition at 200 μM of holo-Rc. In contrast, the apo form even at high concentrations did not have a significant effect on *P. falciparum* growth. These data fully corroborate previous observations using NMR or ITC as much as apo-Rc is unable to bind to MSP1₁₉.

In order to discard that such a parasitemia inhibition could be ascribed to the well-known apoptotic role of several cupredoxins (46,47), control experiments were run with the holo- and apo-forms of Pc. Holo-Pc was chosen as it does not bind to MSP1₁₉, as inferred from the herein presented NMR screening (see above), but it is structurally very similar to Rc: the two proteins belong to the Type I blue copper-protein family, with almost identical folding and tetrahedral copper center. Upon addition of either holo- or apo-Pc (25 μM) under the same culture conditions, the *Plasmodium* growth first slightly decays to further reach a constant value until the end of the experiment. So the *Plasmodium* growth does not depend on protein concentration (the percentage of growth is maintained at ca. 70% even at 200 μM Pc), and is practically the same with either holo- or apo-Pc. Altogether these results

indicate that holo-Rc inhibits parasitemia upon specific binding to MSP1₁₉.

DISCUSSION

Proteins from the cupredoxin family have demonstrated antimalarial activity and potential as therapeutic agents (26,27). We have shown here that the cupredoxin rusticyanin interacts with MSP1₁₉ with micromolar *K*_d, forming a well-defined complex. The interaction takes place on the same surface as that targeted by inhibitory antibodies, suggesting that a similar mechanism could take place. Its strength is dependent on the presence and, to a lesser extent, on the oxidation state of the metal center, which is consistent with the need for an intact interaction surface and charge conservation. Furthermore, we have observed the inhibition of *P. falciparum* parasitemia in infected cells where holo-Rc is present as a result of the interaction with MSP1₁₉. However, negligible effect on parasite growth could be observed for apo-Rc and Pc forms.

MSP1₁₉ signals show slow exchange in the presence of the F_{ab} fragments of the inhibitory mAb12.8 and mAb12.10, indicating the kinetic stability of complexes involving MSP1₁₉ with binding affinity constants in the μM to sub-nM range (20). Rc binds specifically with a *K*_d of 2 μM to the interface between the two MSP1₁₉ EGF domains, overlapping the surface recognized by these inhibitory antibodies (20,21), as indicated by our NMR-based mapping. A detailed comparison of MSP1₁₉ bound to either Rc or mAb12.10 and mAb12.8 reveals that the common interacting surfaces are located in the first EGF domain along with the first β-sheet and at the end of the second EGF domain. Interestingly, these regions of MSP1₁₉ form a shallow pocket (Figure 1B) that may have a role in erythrocyte invasion (21). In addition, these residues involved in the formation of protein complexes with MSP1₁₉ are distributed in three segments – His6-Val9, Lys16-Arg22 and Tyr89-Cys95 (numbering according to the *P. yoelii* MSP1₁₉ sequence, Figure 1A) – and they are strongly conserved in different species (21), supporting the idea that this is a functional site. The presence of additional perturbed residues identified in this study may be explained by the flat structure of MSP1₁₉ (5), since perturbations as a result of a

protein-protein interaction may be transferred from one MSP1₁₉ face to the other.

Another point of interest arising from this study is the mode of interaction of MSP1₁₉ with Rc, compared to the interaction with mAbs. The study took as starting point a structural alignment of Rc with the F_{ab} fragment of the non-inhibitory mAb G17.12 whose interaction with MSP1₁₉ has been solved through X-ray crystallography (15). The similarities with the β -barrel, as well as the loops connecting them, are clear (Figure 2). However, the relative orientation between the mAb and MSP1₁₉ does not match that defined for the MSP1₁₉-Rc complex (Figure 11A). In contrast, the models of mAb12.8-MSP1₁₉ and mAb12.10-MSP1₁₉ complexes built by Autore *et al.* (48) using NMR-based docking calculations match well with the Rc-MSP1₁₉ model reported here. In looking for structural similarities between Rc and mAb12.10 with the DaliLite pairwise comparison server, the Z-score 2.8 (Figure 11B and 11C) suggested strong structural similarities, especially in the loops that interact with MSP1₁₉. In this paper, MSP1₁₉ complexes with mAb12.10 and Rc demonstrate (Figure 11) a similar MSP1₁₉ orientation with respect to the other molecule – mAb12.10 or Rc – within each complex. The A1 region of mAb12.10 forms the main interaction with MSP1₁₉, similar to the structurally-related region of Rc, especially at the level of β -strand connecting loops. As proposed by Autore *et al.* (48), a positively-charged electrostatic spot on the antibody surface is required in the interaction and binding to MSP1₁₉. A similar positively-charged area is located on the Rc surface – Lys81 and Lys116 – in the complex interface, as inferred from our docking simulations (Figure 9C). The Rc-MSP1₁₉ interface also involves hydrophobic contacts in the region surrounding the Rc copper center that presumably plays a key role in complex formation, as indicated by the NMR and ITC

experiments. Reduced Rc binds more efficiently MSP1₁₉ than the oxidized form, suggesting that both electrostatic potential properties and protein folding depend on the metal redox state. This effect is even more drastic for apoRc, which is unable to interact with MSP1₁₉.

The practical significance of these observations can be found in the potential antimalarial role of the binding of Rc to MSP1₁₉ on the parasite surface, thereby blocking parasite growth and interfering directly with parasite invasion of red blood cells. In fact, the interaction might sterically interfere with the recognition between MSP1 and an erythrocyte surface molecule or with the proteolytic processing of MSP1, which occurs during invasion and can be inhibited by antibodies binding to MSP1₁₉. Such a role has been shown previously in the drug suramin (49). An alternative hypothesis, based on the fact that MSP1₁₉ is internalized with the malaria parasite during invasion and then trafficked to the food vacuole where it persists until the end of the next intraerythrocytic cycle (10), is that MSP1₁₉-bound Rc would be internalized and interfere with MSP1₁₉ functioning inside the cell, as shown for an antibody (11). Supporting this possibility, it has been reported that Rc is not only able to enter mammalian cells, but also to induce caspase-8 mediated apoptosis and/or to inhibit the cell cycle (47). Furthermore and unlike other cupredoxins, Rc is a copper protein with high acid stability and is biologically functional at a pH below 1.0 (50). The extreme acid stability of Rc may be important in understanding its function of blocking MSP1₁₉ since pH is approximately 4.5-5.5 inside the *Plasmodium* food vacuole. Altogether, Rc could be an excellent therapeutic tool for malaria treatment and expand our understanding of MSP1₁₉ function. In this way, as well, it could provide beneficial information for drug design.

REFERENCES

1. Hobbs, C., and Duffy, P. (2011) Drugs for malaria: something old, something new, something borrowed. *FI000 Biol. Rep.* **3**, 24.
2. Wells, T. N. C., Alonso, P. L., and Gutteridge, W. E. (2009) New medicines to improve control and contribute to the eradication of malaria. *Nat. Rev. Drug Discov.* **8**, 879-891.
3. Opar, A. (2011) Quarter-century quest for malaria vaccine shows signs of success. *Nat. Rev. Drug Discov.* **10**, 887-888.
4. Holder, A. A. (2009a) Malaria Vaccines: Where Next? *PLoS Pathog.* **5**, e1000638.
5. Holder, A. A. (2009b) The carboxy-terminus of merozoite surface protein 1: structure, specific antibodies and immunity to malaria. *Parasitology.* **136**, 1445-1456.
6. Holder, A.A., and Blackman, M.J. (1994) What is the function of MSP-1 on the malaria merozoite? *Parasitology.* **10**, 182-184.
7. Blackman, M. J., Heidrich, H. G., Donachie, S., McBride, J. S., and Holder, A. A. (1990) A single fragment of a malaria merozoite surface protein remains on the parasite during red cell invasion and is the target of invasion-inhibiting antibodies. *J. Exp. Med.* **172**, 379-382.
8. Blackman, M.J., Ling, I., Nicholls, S.C., and Holder, A.A. (1991) Proteolytic processing of the *Plasmodium falciparum* merozoite surface protein-1 produces a membrane-bound fragment containing two epidermal growth factor-like domains. *Mol. Biochem. Parasitol.* **49**, 29-34.
9. Blackman, M.J., Whittle, H., and Holder, A.A. (1991) Processing of the *Plasmodium falciparum* major merozoite surface protein-1: identification of a 33-kilodalton secondary processing product which is shed prior to erythrocyte invasion. *Mol. Biochem. Parasitol.* **49**, 35-44.
10. Dluzewski, A. R., Ling, I. T., Hopkins, J. M., Grainger, M., Margos, G., Mitchell, G. H., Holder, A.A., and Bannister, L. H. (2008) Formation of the Food Vacuole in *Plasmodium falciparum*: A Potential Role for the 19 kDa Fragment of Merozoite Surface Protein 1 (MSP1₁₉). *PLoS ONE.* **3**, e3085.
11. Moss, D. K., Remarque, E. J., Faber, B. W., Cavanagh, D. R., Arnot, D. E., Thomas, A. W., and Holder, A. A. (2012) *Plasmodium falciparum* merozoite surface protein (MSP) 119-specific antibodies that interfere with parasite growth in vitro can inhibit MSP1 processing, merozoite invasion and intracellular parasite development. *Infect. Immun.* **80**, 1280-1287.
12. Morgan, W.D., Birdshall, B., Frenkiel, T.A., Gradwell, M.G., Burghaus, P.A., Syed, S.E. H., Uthaiipull, C., Holder, A.A., and Freney, J. (1999) Solution structure of an EGF module pair from the *Plasmodium falciparum* merozoite surface protein-1. *J. Mol. Biol.* **289**, 113-122.
13. Garman, S. C., Simcoke, W. N., Stowers, A. W., and Garboczi, D. N. (2003) Structure of the C-terminal domains of merozoite surface protein-1 from *Plasmodium knowlesi* reveals a novel histidine binding site. *J. Biol. Chem.* **278**, 7264-7269.
14. Babon, J. J., Morgan, W. D., Kelly, G., Eccleston, J. F., Feeney, J., and Holder, A. A. (2007) Structural studies on *Plasmodium vivax* merozoite surface protein-1. *Mol. Biochem. Parasitol.* **153**, 31-40.
15. Pizarro, J. C., Chitarra, V., Verger, D., Holm, I., Pêtres, S., Dartevelle, S., Nato, F., Longacre, S., and Bentley, G. A. (2003) Crystal structure of a Fab complex formed with PfMSP1-19, the C-terminal fragment of merozoite surface protein 1 from *Plasmodium falciparum*: a malaria vaccine candidate. *J. Mol. Biol.*, **328**, 1091-1103.
16. Chitarra, V., Holm, I., Bentley, G. A., Pêtres, S., and Longacre, S. (1999) The crystal structure of C-terminal merozoite surface protein 1 at 1.8 Å resolution, a highly protective malaria vaccine candidate. *Mol. Cell* **3**, 457-464.
17. O'Donnell, R. A., Saul, A., Cowman, A. F., and Crabb, B. S. (2000) Functional conservation of the malaria vaccine antigen MSP-119 across distantly related *Plasmodium* species. *Nat. Med.* **6**, 91-95.

18. Larkin, M. A., Blackshields, G., Brown, N. P., Chenna, R., McGettigan, P. A., McWilliam, H., Valentin, F., Wallace, I.M., Wilm, A., Lopez, R., Thomson, J.D., Gibson, T.J., and Higgins, D. G. (2007) Clustal W and Clustal X version 2.0. *Bioinformatics* **23**, 2947-2948.
19. Hensmann, M., Li, C., Moss, C., Lindo, V., Greer, F., Watts, C., Ogun, S.A., Holder, A.A., and Langhorne, J. (2004) Disulphide bonds in merozoite surface protein 1 of the malaria parasite impede efficient antigen processing and affect the *in vivo* antibody response. *Eur. J. Immunol.* **34**, 639-648.
20. Morgan, W.D., Lock, M.J., Frenkiel, T.A., Grainger, M., and Holder, A.A. (2004) Malaria parasite-inhibitory antibody epitopes on *Plasmodium falciparum* merozoite surface protein-119 mapped by TROSY NMR. *Mol. Biochem. Parasitol.* **138**, 29-36.
21. Morgan, W. D., Frenkiel, T. A., Lock, M. J., Grainger, M., and Holder, A. A. (2005) Precise epitope mapping of malaria parasite inhibitory antibodies by TROSY NMR Cross-Saturation. *Biochemistry.* **44**, 518-523.
22. Ling, I. T., Ogun, S. A., and Holder, A. A. (1994) Immunization against malaria with a recombinant protein. *Parasite Immunol.* **16**, 63-67.
23. Spencer Valero, L. M., Ogun, S. A., Fleck, S. L., Ling, I. T., Scott-Finnigan, T. J., Blackman, M. J., and Holder, A. A. (1998) Passive immunization with antibodies against three distinct epitopes on *Plasmodium yoelii* merozoite surface protein 1 suppresses parasitemia. *Infect. Immun.* **66**, 3925-3930.
24. Benjamin, P. A., Ling, I. T., Clottey, G., Spencer Valero, L. M., Ogun, S. A., Fleck, S. L., Walliker, D., Morgan, W. D., Birdsall, B., Feeney, J., and Holder, A. A. (1999) Antigenic and sequence diversity at the C-terminus of the merozoite surface protein-1 from rodent malaria isolates, and the binding of protective monoclonal antibodies. *Mol. Biochem. Parasitol.* **104**, 147-156.
25. Lazarou, M., Patiño, J. A.G., Jennings, R. M., McIntosh, R. S., Shi, J., Howell, S., Cullen, E., Jones, T., Adame-Gallegos, J.R., Chappel, J.A., McBride, J.S., Blackman, M.J., Holder A.A., and Pleass, R. J. (2009) Inhibition of erythrocyte invasion and *Plasmodium falciparum* merozoite surface protein 1 processing by human immunoglobulin G1 (IgG1) and IgG3 antibodies. *Infect. Immun.* **77**, 5659-5667.
26. Chaudhari, A., Fialho, A. M., Ratner, D., Gupta, P., Hong, C. S., Kahali, S., Yamada, T., Haldar, K., Cho, W., Chauhan, V. S., Das Gupta, T. K., and Chakrabarty, A. M. (2006) Azurin, *Plasmodium falciparum* Malaria and HIV/AIDS: Inhibition of parasitic and viral growth by azurin. *Cell Cycle.* **5**, 1642-1648.
27. Chakrabarty, A.M., Gupta, T.K.D., Yamada, T., Chaudhari, A., Fialho, A.M., and Hong, C.S. (2006) Composition and methods for treating malaria with cupredoxin and cytochrome. USA Patent Office WO 2006/127477 A3.
28. Hasegawa, H., and Holm, L. (2009) Advances and pitfalls of protein structural alignment. *Curr. Opin. Struct. Biol.* **19**, 341-348.
29. Morgan, W.D., Kragt, A., and Feeney, J. (2000) Expression of deuterium-isotope-labelled protein in the yeast *Pichia pastoris* for NMR studies. *J. Biomol. NMR.* **17**, 337-347.
30. Jiménez, B., Piccioli, M., Moratal, J.M., and Donaire, A. (2003) Backbone dynamics of rusticyanin: the high hydrophobicity and rigidity of this blue copper protein is responsible for its thermodynamic properties. *Biochemistry.* **42**, 10396-10405.
31. Hall, J.F., Hasnain, S.S., and Ingledew, W.J. (1996) The structural gene for rusticyanin from *Thiobacillus ferrooxidans*: cloning and sequencing of the rusticyanin gene. *FEMS Microbiol. Lett.* **137**, 85-89.
32. Díaz-Moreno, I., Díaz-Quintana, A., De la Rosa, M. A., and Ubbink, M. (2005) Structure of the complex between plastocyanin and cytochrome *f* from the cyanobacterium *Nostoc* sp. PCC 7119 as determined by paramagnetic NMR. *J. Biol. Chem.* **280**, 18908-18915.
33. Crowley, P. B., Otting, G., Schlarb-Ridley, B. G., Canters, G. W., and Ubbink, M. (2001) Hydrophobic interactions in a cyanobacterial plastocyanin–cytochrome *f* complex. *J. Am. Chem. Soc.* **123**, 10444-10453.

34. Lange, C., Cornvik, T., Díaz-Moreno, I., and Ubbink, M. (2005) The transient complex of poplar plastocyanin with cytochrome *f*: effects of ionic strength and pH. *Biochim. Biophys. Acta.* **1707**, 179-188.
35. Van de Kamp, M., Hali, F. C., Rosato, N., Agro, F.A., and Canters, G. W. (1990) Purification and characterization of a non-reconstitutable azurin, obtained by heterologous expression of the *Pseudomonas aeruginosa* *azu* gene in *Escherichia coli*. *Biochim. Biophys. Acta.* **1019**, 283-292.
36. Goddard, T. D., and Kneller, D. G. (2006) SPARKY 3. University of California, San Francisco.
37. Palma, P. N., Krippahl, L., Wampler, J. E., and Moura, J. J. G. (2000) BiGGER: A new (soft) docking algorithm for predicting protein interactions. *Proteins* **39**, 372-384.
38. Crane, B.R., Di Bilio, A.J., Winkler, J.R., and Gray, H.B. (2001) Electron tunneling in single crystals of *Pseudomas aeruginosa* azurins. *J. Am. Chem. Soc.* **123**, 11623-11631.
39. Badsberg, U., Jorgensen, A.M., Gesmar, H., Led, J.J., Hammerstad, J.M., Jespersen, L.L., and Ulstrup, J. (1996) Solution structure of reduced plastocyanin from the blue- green alga *Anabaena variabilis*. *Biochemistry.* **35**, 7021-7031.
40. Zhao, D. and Shoham, M. (1998) Rusticyanin: extremes in acid stability and redox potential explained by the crystal structure. *Biophys. J.* **74**, 233.
41. Pettersen, E.F., Goddard, T.D., Huang, C.C., Couch, G.S., Greenblatt, D.M., Meng, E.C., and Ferrin, T.E. (2004) UCSF Chimera – a visualization system for exploratory research and analysis. *J. Comput. Chem.* **25**, 1605-1612.
42. Alcaraz, L. A., and Donaire, A. (2005) Rapid binding of copper(I) to folded aporusticyanin. *FEBS Lett.* **579**, 5223-5226.
43. Zaballa, M. E., Abriata, L. A., Donaire, A., and Vila, A.J. (2012) Flexibility of the metal-binding region in apo-cupredoxins. *Proc. Natl. Acad. Sci. USA* **109**, 9254-9259
44. Cruz-Gallardo, I., Díaz-Moreno, I., Díaz-Quintana, A., and De la Rosa, M. A. (2012) The cytochrome *f*- plastocyanin complex as a model to study transient interactions between redox proteins. *FEBS Lett.* **586**, 646-652.
45. Díaz-Moreno, I., Díaz-Quintana, A., Molina-Heredia, F.P., Nieto, P.M., Hansson, Ö., De la Rosa, M. A., and Karlsson, G.B. (2005) NMR analysis of the transient complex between membrane photosystem I and soluble cytochrome *c*₆. *J. Biol. Chem.* **280**, 7925-7931.
46. Yamada, T., Goto, M., Punj, V., Zaborina, O., Kimbara, K., Das Gupta, T. K., and Chakrabarty, A. M. (2002) The bacterial redox protein azurin induces apoptosis in J774 macrophages through complex formation and stabilization of the tumor suppressor protein p53. *Infect. Immun.* **70**, 7054-7062.
47. Yamada, T., Hiraoka, Y., Gupta, T. K. D., and Chakrabarty, A. M. (2004) Rusticyanin, a bacterial electron transfer protein, causes G1 arrest in J774 and apoptosis in human cancer cells. *Cell Cycle* **3**, 1182-1187.
48. Autore, F., Melchiorre, S., Kleinjung, J., Morgan, W. D., and Fraternali, F.(2007) Interaction of malaria parasite-inhibitory antibodies with the merozoite surface protein MSP119 by computational docking. *Proteins* **66**, 513-527.
49. Fleck, S. L., Birdsall, B., Babon, J., Dluzewski, A. R., Martin, S. R., Morgan, W. D., Angov, E., Kettleborough, C. A., Feeney, J., Blackman, M. J., and Holder, A. A. (2003) Suramin and suramin analogues inhibit merozoite surface protein-1 secondary processing and erythrocyte invasion by the malaria parasite *Plasmodium falciparum*. *J. Biol. Chem.* **278**, 47670-47677.
50. Blake II R.C. and Shute E.A. (1987) Respiratory enzymes of *Thiobacillus ferrooxidans*. A kinetic study of electron transfer between iron and rusticyanin in sulfate media. *J. Biol. Chem.* **262**, 14983-14989.

Acknowledgements - The authors wish to thank G. Kelly (London, UK) for his support on recording NMR experiments and Dr. F. Fraternali (London, UK) for providing the coordinates of MSP1₁₉ in complex with inhibitory antibodies (12.8 and 12.10). Aliquots of azurin were kindly supplied by Prof. M. Ubbink (Leiden, The Netherlands).

FOOTNOTES

* This work was supported by Junta de Andalucía (P08-CVI-3876 and BIO198) (Spain); European Social Fund-ERDF (2007-2013). Isabel Cruz-Gallardo was funded by a PhD grant of the Junta de Andalucía (P08-CVI-3876) and GERMN bursaries for short-term stays (Spain). Antonio Donaire was funded by Ministerio de Economía y Competitividad (SAF2011-26611) and Fundación Séneca de la Región de Murcia (15354/PI/10) (Spain). Adrián Velázquez-Campoy was supported by grant BFU2010-19451 from Ministerio de Ciencia e Innovación (Spain). Work in the Holder laboratory was funded by the MRC (U117532067) and EU FP7 Network of Excellence EviMalar. Rachel D.Curd received an MRC Studentship. Andres Ramos was funded by the MRC (U117574558).

⁶The abbreviations used are: MSP1, merozoite surface protein 1; GPI, glycosyl phosphatidyl inositol; MSP1₁₉, merozoite surface protein 1-19; EGF, epidermal growth factor; mAbs, monoclonal antibodies; ITC, isothermal titration calorimetry; BiGGER, bimolecular complex generation with global evaluation and ranking; Rc, rusticyanin, Pc, plastocyanin; Az, azurin; HSQC, Heteronuclear single-quantum coherence; TOCSY, total correlation spectroscopy; K_d , dissociation constant.

FIGURE LEGENDS

FIGURE 1. MSP1₁₉ protein. (A) Multiple sequence alignment of MSP1₁₉ with ClustalW2 (18) from a number of *Plasmodium* species. Sequences are colored by percent identity: black (100%), dark grey (80%), light grey (60%) and white (<50%). Secondary structure elements of *P. yoelii* MSP1₁₉ are shown. Orange boxes highlight cysteine residues that are conserved across different *Plasmodium* species, whereas red boxes highlight those present only in *P. falciparum*. Gold arrows stand for disulphide bonds formed by cysteine residues. The main difference between *P. falciparum* MSP1₁₉ and homologues from other *Plasmodium* species characterized to date lies in the disulphide-bond pattern of the protein from the other species: one of the cysteine pairs in the first EGF domain is substituted by a tryptophan and a non-polar or aliphatic residue. (B) Ribbon representation of the lowest energy NMR structure of *P. yoelii* MSP1₁₉ (BMRB accession number: 19233). Side-chains of cysteine residues forming disulphide bridges are represented in gold.

FIGURE 2. Conserved structural motifs. (A) Ribbon representation of the F_{ab} fragment of G17.12 monoclonal Antibody (mAb; 1OB1.pdb). Domain A is depicted in light grey and domain B in gold. (B) Structural alignment of Az (*upper*, 1JZG.pdb) and A1 fragment of F_{ab} (*lower*) built by DaliLite pairwise comparison server. Matching regions - with a Dali Z-score of 2.9 - appear in orange. (C) Ribbon representation of Rc (*upper*, 1A3Z.pdb) and Pc (*lower*, 1NIN.pdb). Dali Z-scores for Rc and Pc are 2.6 and 3.1, respectively. Copper atoms are colored in blue.

FIGURE 3. *Ab initio* docking of cupredoxins with MSP1₁₉ performed by BiGGER. *Left* - Az. *Center* - Pc. *Right* - Rc. Light yellow spheres represent the geometry centers of MSP1₁₉ in the 100 best solutions generated for each complex. All cupredoxins are oriented with respect to their copper center. Robertson diagrams of the cupredoxins are colored according to secondary

structures: α helices in red and β strands in blue. Copper atoms are represented as blue spheres and the residues bonding to them are in grey sticks.

FIGURE 4. NMR titrations of ¹⁵N MSP1₁₉ with reduced cupredoxins. *Upper* - Az from *Pseudomonas aeruginosa*. *Middle* - Pc from *Nostoc* sp. PCC 7119. *Lower* - Rc from *Acidithiobacillus ferrooxidans*. Superimposition of ¹⁵N HSQC spectra of free MSP1₁₉ (magenta) and after adding one out of three cupredoxins (blue) at a cupredoxin:MSP1₁₉ ratio of 4:1. Arrows point out those residues which experience substantial broadening. Negligible binding to MSP1₁₉ was observed upon adding aliquots of Pc and Az.

FIGURE 5. NMR titration of ¹⁵N MSP1₁₉ with reduced Rc. (A) ¹⁵N linewidth differences (¹⁵N $\Delta\Delta v_{1/2\text{Binding}}$) between free and Rc-bound MSP1₁₉. The Rc:MSP1₁₉ ratios are 0.5:1 (red), 1:1 (grey) and 1.5:1 (blue). (B) Superposition of ¹⁵N HSQC spectra of free MSP1₁₉ (magenta) and bound to Rc (blue) in a Rc:MSP1₁₉ ratio of 1.5:1. A subset of three representative resonances is labeled in black. (C) Map of MSP1₁₉ interface upon binding to Rc. MSP1₁₉ surface is rotated 90° around the vertical axes in each view. Residues are colored according to their ¹⁵N $\Delta\Delta v_{1/2\text{Binding}}$ (Hz): the resonances that undergo the largest broadening ($\geq 5\text{Hz}$) are orange and the signals with a significant linewidth over the detection limit $< 5\text{Hz}$ are yellow. The limit of 5 Hz corresponds to a threshold value relative to the average plus 2-fold the standard deviation ($\Delta\Delta v_{1/2\text{Binding}} \geq \langle \Delta\Delta v_{1/2\text{Binding}} \rangle + 2S_{n-1}$). Residues with no linewidth perturbation are marked in blue, whereas prolines are in grey.

FIGURE 6. Comparison between NMR titrations of ¹⁵N MSP1₁₉ with either oxidized or reduced Rc at Rc:MSP1₁₉ ratio of 4:1. Most of the MSP1₁₉ signals in binding to Rc(Cu¹⁺) are broadening over the detection limit at the Rc:MSP1₁₉ ratio of 4:1, suggesting that MSP1₁₉ binds reduced Rc with a higher affinity. (A) *Upper*: Overlap between ¹⁵N HSQC spectra of free MSP1₁₉ (magenta) and oxidized Rc-bound MSP1₁₉ (blue). *Lower*: Map of MSP1₁₉ in the presence of oxidized Rc. (B) The same as 6A with reduced Rc. The 90°-rotated surface representations of MSP1₁₉ show residues colored according their ¹⁵N $\Delta\Delta v_{1/2\text{Binding}}$ following the same color-code as in Figure 5C. Those residues broadened beyond the detection limit are highlighted in red.

FIGURE 7. ITC titrations of MSP1₁₉ with both redox states of Rc. Binding assays of the complexes between MSP1₁₉ and reduced (*left*) or oxidized Rc (*right*). Thermograms are shown at the top and binding isotherms at the bottom, along with the dissociation constant (K_d expressed in μM), enthalpy (ΔH in kcal/mol). The stoichiometry value (n) was fixed to avoid degeneracy in the non-linear regression data analysis. Typical relative errors are 20-25% for the dissociation constant and 5-10% for the stoichiometry.

FIGURE 8. NMR and ITC titrations of MSP1₁₉ with apo-Rc. (A) ¹⁵N linewidth differences (¹⁵N $\Delta\Delta v_{1/2\text{Binding}}$) between free MSP1₁₉ and in the presence of apo-Rc. The apo-Rc:MSP1₁₉ ratios were 1:1 (red), 1.5:1 (grey) and 4:1 (blue). (B) Overlap between ¹⁵N HSQC spectra of free MSP1₁₉ (magenta) and in the presence of apo-Rc (blue) at an apo-Rc:MSP1₁₉ ratio of 4:1. (C) ITC thermogram obtained from the apo-Rc-MSP1₁₉ titration, revealing the lack of binding between both proteins, because of the flat calorimetric profile.

FIGURE 9. BIGGER molecular docking of the MSP1₁₉-Rc complex. (A) *Left* - Best 100 models with the lowest energy values after alignment of MSP1₁₉ molecules with Rc geometry centers represented by spheres. Ribbon (*center*) and space-filling (*right*) representations for the best model are shown in the same orientation as on the *left*. MSP1₁₉ is represented in dark grey whereas Rc is in light blue. (B) Interface residues of the MSP1₁₉/Rc complex. MSP1₁₉ and Rc are independently rotated 90° to the top and to the bottom, respectively, with regard to their orientation in A. Contacting residues are depicted in light yellow for the MSP1₁₉ and dark blue for Rc. (C) Electrostatic potential surfaces of MSP1₁₉ (*upper*) and Rc (*lower*) with the same orientations as in B. The electrostatic potential surfaces were created with a color ramp for

positive (blue) and negative (red) potentials at 300 mM ionic strength. The potentials were calculated in Chimera software (41).

FIGURE 10. Inhibition of *P. falciparum* growth by Rc. Percentage of parasite growth was measured in the presence of either holo-Rc (filled circles), apo-Rc (open circles), holo-Pc (filled stars) or apo-Pc (open stars) at varying concentration (see Experimental Procedures). Parasite cultures were incubated with the Rc or Pc forms for a 96 h-period, with a medium change after 48 hours. Cultures in the absence of cupredoxin were used as a positive control.

FIGURE 11. Comparison of complexes containing MSP1₁₉. (A) MSP1₁₉/mAbG17.12 crystallographic structure (1OB1.pdb; 15). Domain A1 of the non-inhibitory mAbG17.12 is represented in light grey, whereas *P. falciparum* MSP1₁₉ is in purple. (B) MSP1₁₉/mAb12.10 complex, whose PDB coordinates were kindly provided by Fraternali and coworkers (48). Domain A1 of the inhibitory mAb12.10 and *P. falciparum* MSP1₁₉ were colored as in A. (C) MSP1₁₉/Rc complex studied in this work. *P. yoelii* MSP1₁₉ is depicted in dark grey and Rc in light blue. Copper center is represented by a blue sphere. Matching regions between mAbG17.12 or mAb12.10 and Rc after structural alignment using DaliLite were depicted in orange. The 180°-rotated views for both MSP1₁₉/mAb12.10 and MSP1₁₉/Rc complexes are shown.

TABLE 1. Thermodynamic values inferred from ITC experiments.

MSP1 ₁₉ complex	ΔG (kcal/mol)	ΔH (kcal/mol)	$-T\Delta S$ (kcal/mol)	K_d (μM)
Oxidized Rc	-6.8	15	-21.8	20
Reduced Rc	-8.4	-1.7	-6.7	2

The affinity of a protein-protein interaction is defined by the Gibbs energy of the binding: $\Delta G = -RT \ln K_d$. ΔG has two different contributions, ΔH and ΔS , according to the equation: $\Delta G = \Delta H - T\Delta S$, thus several combinations of those values could yield similar binding affinities. The complex formation is entropically driven in both cases, being the enthalpic contribution to the binding unfavorable (15 kcal/mol with oxidized Rc) or only slightly favorable (-1.7 kcal/mol with reduced Rc).

Figure 1

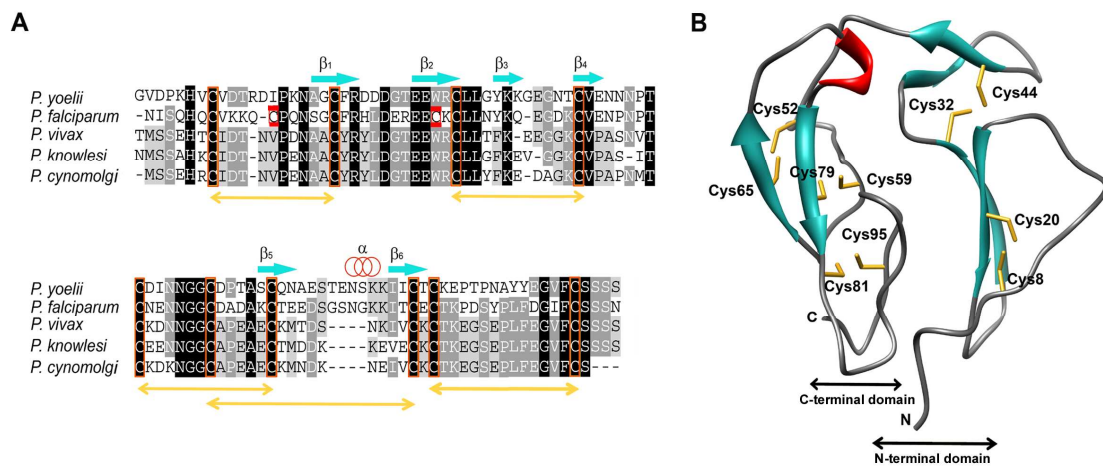


Figure 2

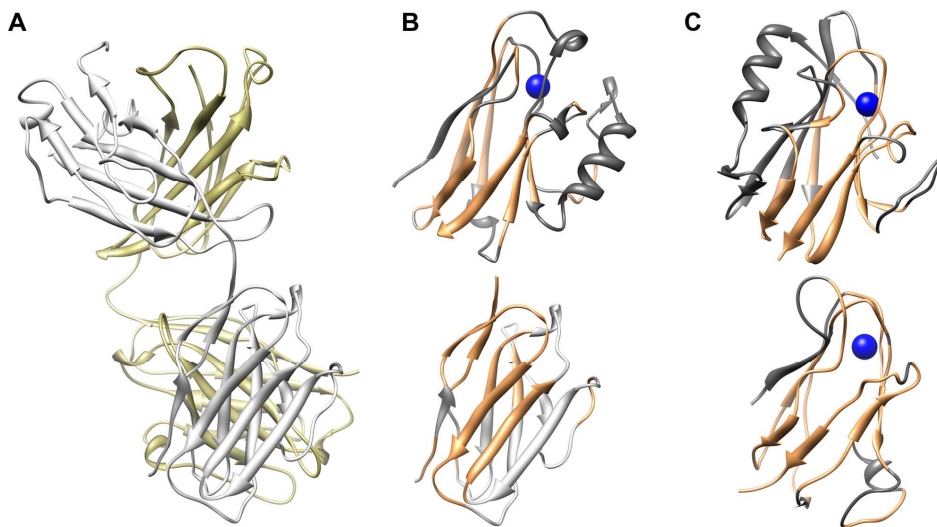


Figure 3

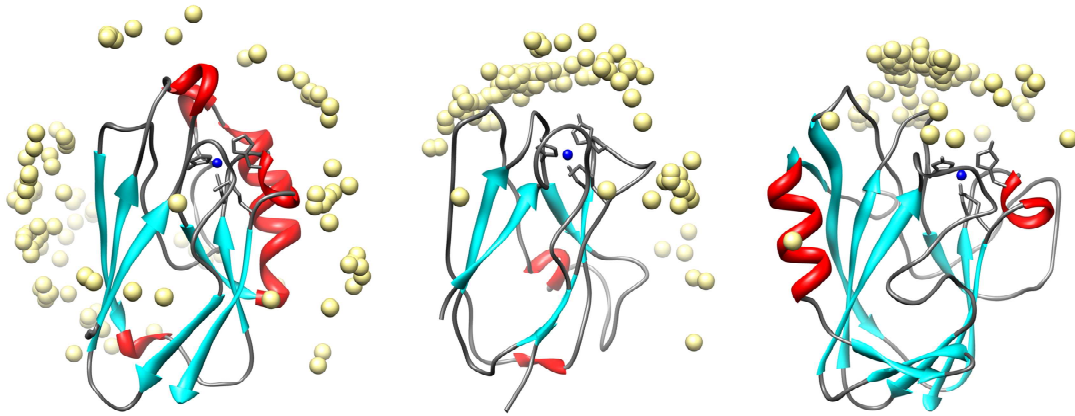


Figure 4

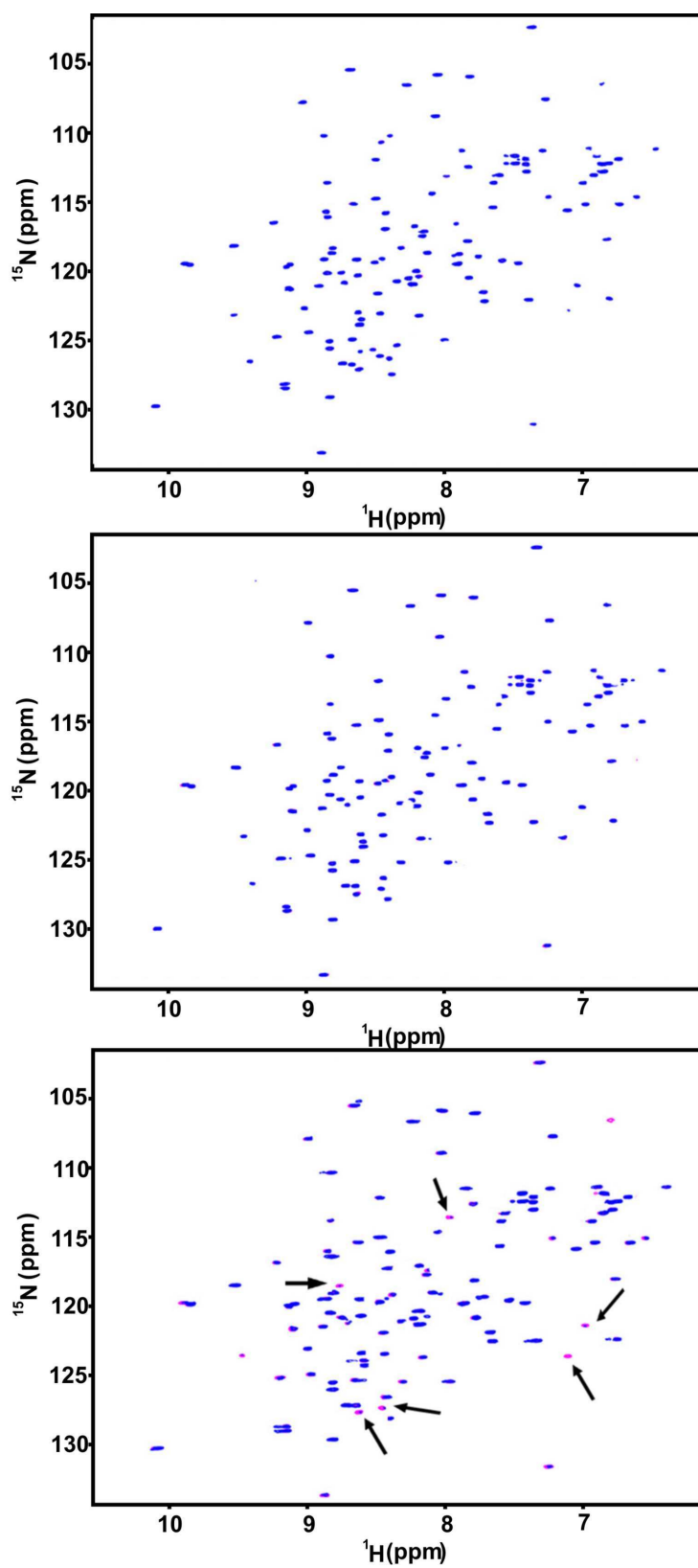


Figure 5

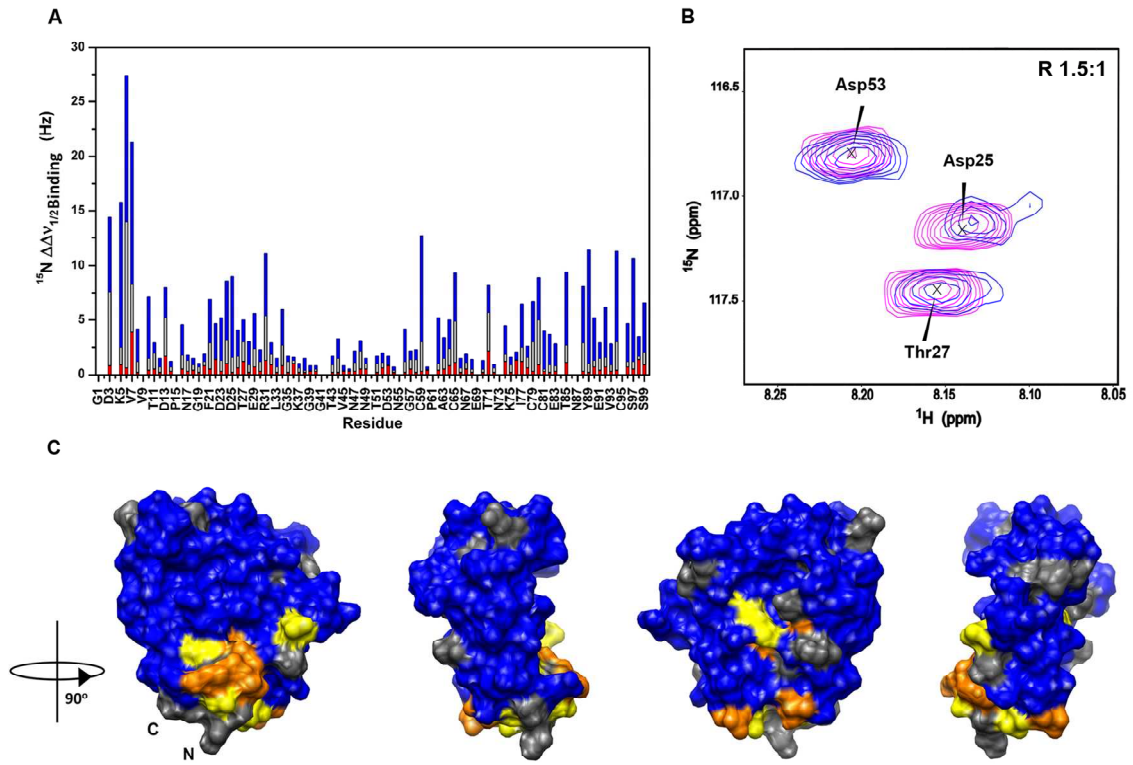


Figure 6

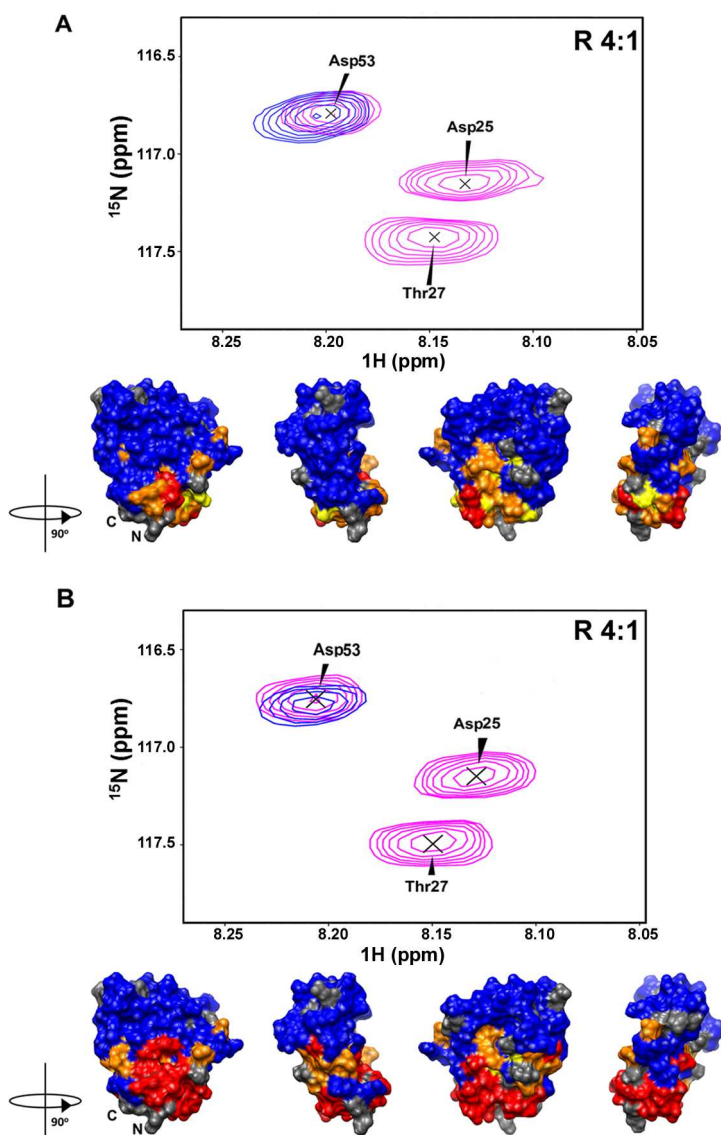


Figure 7

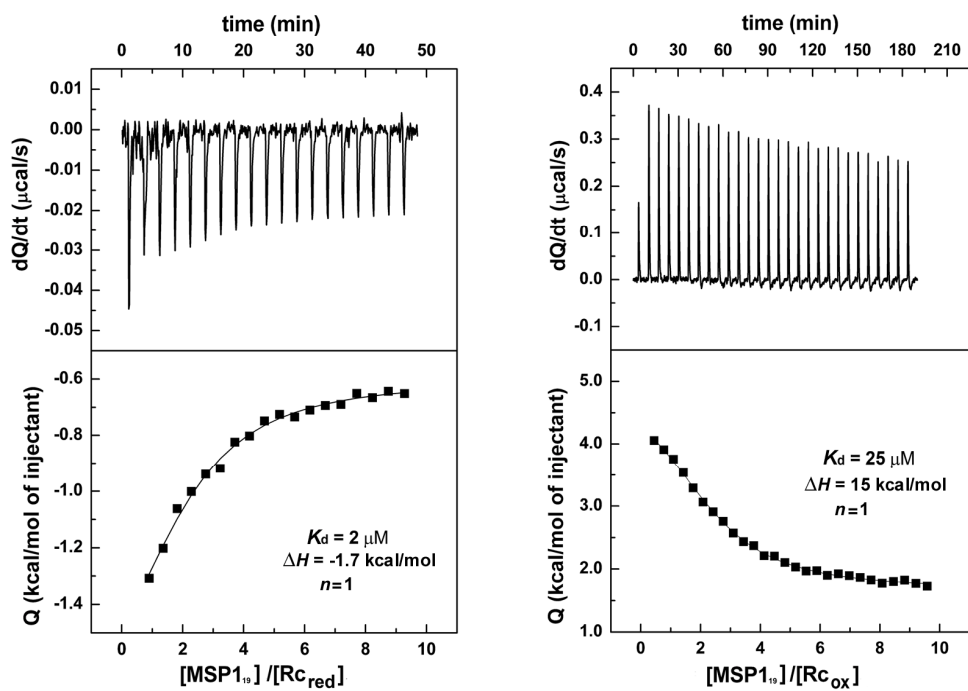


Figure 9

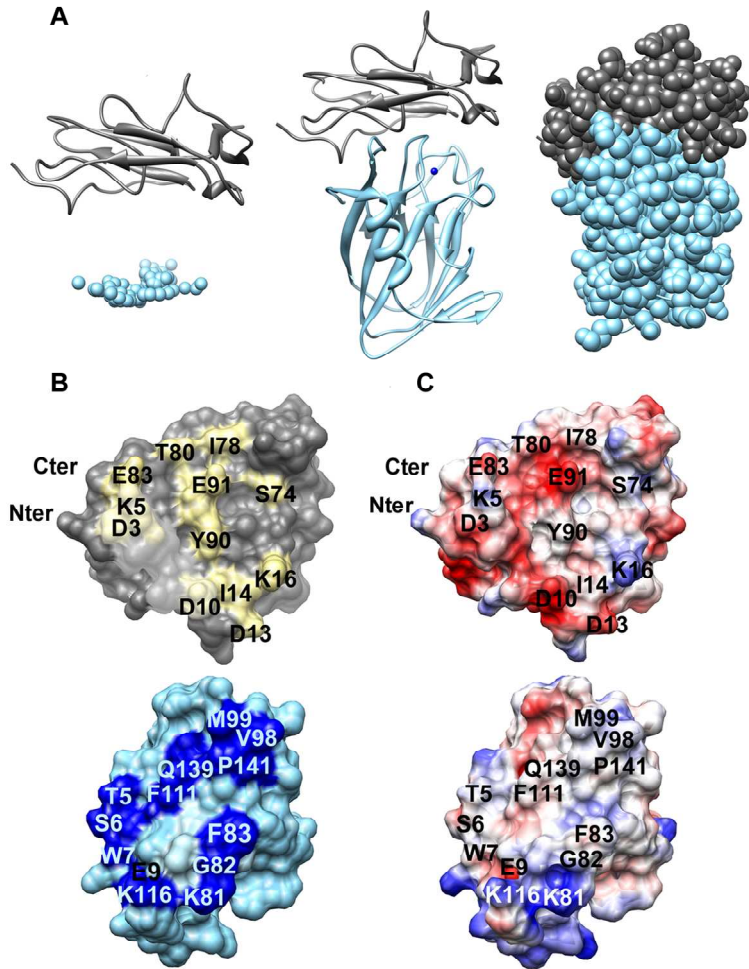


Figure 10

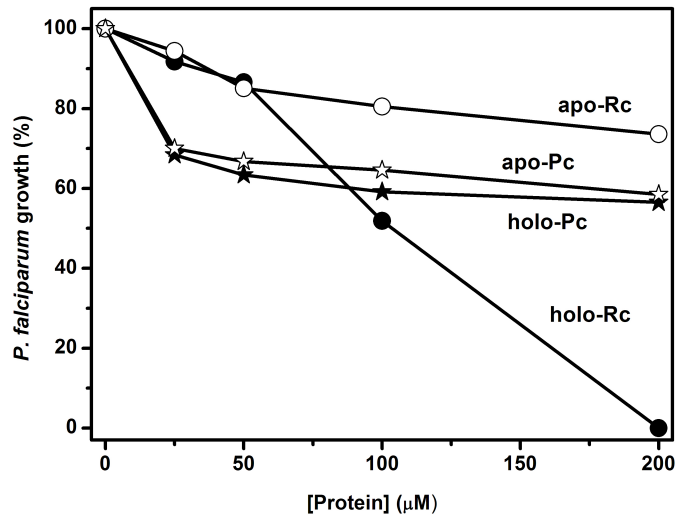


Figure 11

